

Shell Structure of Confined Charges at Strong Coupling

J. Wrighton,¹ J. Dufty,¹ M. Bonitz,² and H. Kählert²

¹*Department of Physics, University of Florida, Gainesville, FL 32611*

²*Institut für Theoretische Physik und Astrophysik,*

Christian-Albrechts Universität zu Kiel, 24098 Kiel, Germany

(Dated: October 22, 2018)

Abstract

A theoretical description of shell structure for charged particles in a harmonic trap is explored at strong coupling conditions of $\Gamma = 50$ and 100 . The theory is based on an extension of the hypernetted chain approximation to confined systems plus a phenomenological representation of associated bridge functions. Predictions are compared to corresponding Monte Carlo simulations and quantitative agreement for the radial density profile is obtained.

PACS numbers:

Systems of harmonically trapped charged particles exhibit a shell structure in their radial density profile. Recent studies [1, 2, 3, 4, 5, 6], both experimental and molecular dynamics simulation, indicate the localization of the charges on the surfaces of concentric spheres with a crystal-like ordering on each surface depending on the particle number N . These are effectively the zero temperature ground state for the system or energetically close excited states. An accurate and instructive theoretical description of these spherical crystals has been given recently using shell models [6, 7, 8]. A complementary theoretical description of the fluid phase at finite temperatures has now been given as well [9], showing a closely related "blurred" shell structure that sharpens at stronger Coulomb coupling $\Gamma \equiv q^2/r_0k_B T$ (q is the charge, r_0 is the ion sphere radius in terms of the average trap density). This fluid phase theory demonstrates that correlations play the dominant role in the formation of shell structure. An extension of the hypernetted chain approximation (HNC) for bulk fluids to the localized charges of a trap was shown to provide all of the qualitative features of shell structure (e.g., number and location of density peaks, shell populations) for the Coulomb coupling constant $\Gamma \geq 10$. However, comparison with Monte Carlo (MC) simulation results at selected conditions showed significant errors in the HNC amplitudes and widths of the shells (20 – 40%). An adjusted HNC (AHNC) was proposed to correct these deficiencies, using a phenomenological representation of the neglected "bridge functions". Excellent agreement with MC results was obtained in this way for $\Gamma = 20, N = 25, 100$ and $\Gamma = 40, N = 300$. The objective here is to report further exploration of the AHNC at the stronger coupling values $\Gamma = 50$ and 100 , and to note some interesting similarities to the crystal shell structure.

The origin of the AHNC theory for confined systems is summarized briefly first. Consider a system of N classical charges in an external potential. The Hamiltonian for this system is

$$H = H_0 + \sum_{i=1}^N V_0(\mathbf{r}_i), \quad H_0 = \sum_{i=1}^N \frac{1}{2} m v_i^2 + \frac{1}{2} \sum_{i \neq j=1}^N V(r_{ij}) \quad (1)$$

where \vec{r}_i and \vec{v}_i are the position and velocity of charge i . The external potential seen by each particle is denoted by $V_0(r)$, and the interaction between the pair i, j is $V(r_{ij})$ (application here will be limited to Coulomb interactions but the discussion is more general). The external potential induces a non-uniform equilibrium density $n(\mathbf{r})$. It follows from density functional

theory that $n(\mathbf{r})$ obeys the equation [10]

$$\ln \frac{n(\mathbf{r})\lambda^3}{z} = -\beta V_0(\mathbf{r}) - \beta \frac{\delta F_{ex}(\beta | n)}{\delta n(\mathbf{r})}, \quad (2)$$

where $z = e^{\beta\mu}$, μ is the chemical potential, and $\lambda = (h^2\beta/2\pi m)^{1/2}$ is the thermal wavelength. The excess free energy $F_{ex}(\beta | n)$ is a universal functional of the density for the Hamiltonian H_0 , independent of the applied external potential V_0 , and describes all correlations among the particles. The solutions to (2) are such that there is a unique equilibrium density $n(\mathbf{r})$ for each $V_0(\mathbf{r})$, using the same $F_{ex}(\beta | n)$. A special case is the uniform density of a one component plasma (OCP), resulting from the $V_0(\mathbf{r})$ for a uniform neutralizing background. The quite different non-uniform density of interest here results from the harmonic trap $V_0(\mathbf{r}) = m\omega^2 r^2/2$. (The spherical symmetry of V_0 in both cases yields a spherically symmetric density profile in the fluid phase; the broken symmetry crystal profile is not considered here).

This observation that the OCP and trap densities are determined from the same excess free energy functional opens the possibility of describing correlations for the trap in terms of those of the OCP. This is done in reference [9] with the result

$$\ln \frac{n(r)\lambda^3}{z} = -\beta \frac{1}{2} m\omega^2 r^2 + \beta \int d\vec{r}' n(r') c_{\text{OCP}}(|\vec{r} - \vec{r}'|; \Gamma) + B_{\text{T}}(r|n) \quad (3)$$

where c_{OCP} is the direct correlation function of a one-component plasma, and $B_{\text{T}}(r|n)$ is the ‘‘bridge function’’ for the trapping potential. The Ornstein-Zernicke equation relates c_{OCP} to the pair distribution function for the OCP, g_{OCP} . A similar analysis gives an equation for g_{OCP}

$$\ln g_{\text{OCP}}(r) = -\beta q^2 r^{-1} + \beta \int d\vec{r}' [g_{\text{OCP}}(r') - 1] c_{\text{OCP}}(|\vec{r} - \vec{r}'|; \Gamma) + B_{\text{OCP}}(r|g_{\text{OCP}}). \quad (4)$$

These two equations provide a formally exact description of the charged particle system from which approximations can be made. In particular, the HNC approximation for both the OCP and the trap density is defined by the neglect of both bridge functions in these equations. The trap density is then determined entirely in terms of correlations for the OCP.

The HNC density profile is very accurate at weak to moderate coupling, $\Gamma < 10$, but has significant quantitative errors as the shell structure develops at larger values of the coupling. This is illustrated in Figure 1 for $\Gamma = 30$, $N = 100$. It was proposed in reference

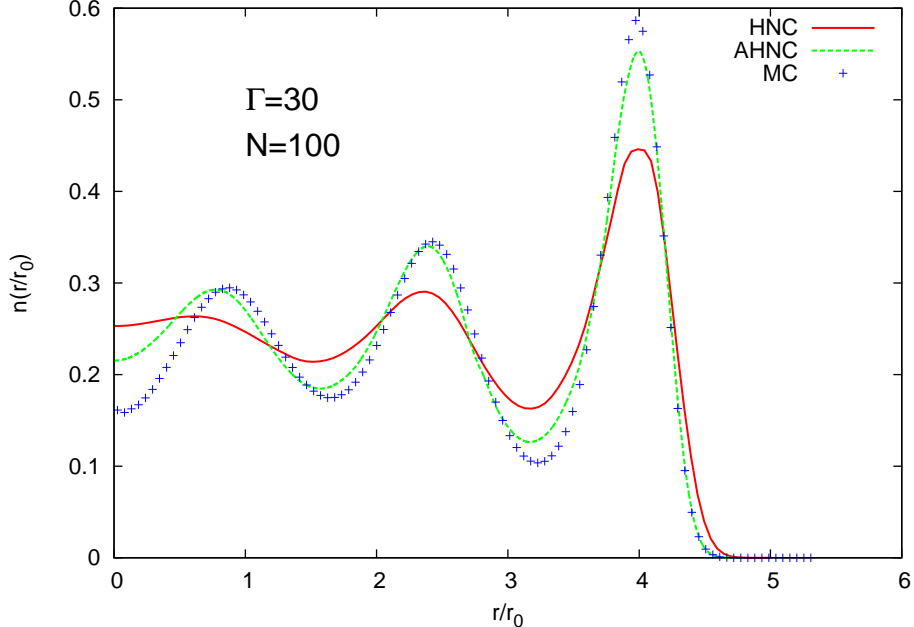


FIG. 1: Comparison of HNC and adjusted HNC (AHNC) to Monte Carlo (MC) results. Conditions are $\Gamma = 30$ and $N = 100$.

[9] to improve the HNC by a phenomenological representation of the bridge functions in the form

$$B(r|n) \rightarrow \lambda(\Gamma)\beta V_0(r), \quad (5)$$

where V_0 is the harmonic potential for B_T or Coulomb potential for B_{OCP} . Also $\lambda(\Gamma)$ is chosen to interpolate between $\lambda(0) = 0$ and some constant $\lambda(\infty)$. This approach was first introduced by Ng [11] for the OCP pair distribution. Subsequently, Rosenfeld and Ashcroft have defined related "modified" HNC approximations using the bridge function as a fitting function [12]. The advantage of the form (5) is that the effect of the bridge functions is to simply "renormalize" the external potential in both eqs. (3) and (4), so that the original HNC approximation is regained except with an effective coupling constant Γ' defined by

$$\Gamma' = [1 + \lambda(\Gamma)] \Gamma \quad (6)$$

In the original work of Ng, he obtained agreement with the Monte Carlo data for g_{OCP} to within a few percent using $\lambda(\infty) = 0.6$. That same value for $\lambda(\infty)$ has been used in reference [9] and in the results presented here.

The improvement gained from this AHNC is also shown in Figure 1. All three curves agree

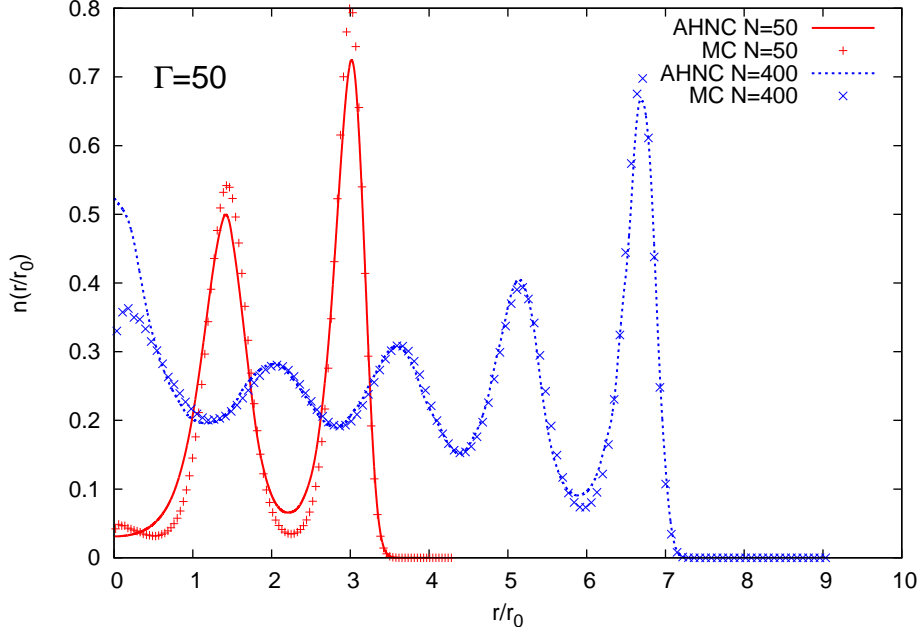


FIG. 2: Comparison of density profile for AHNC and MC, for $\Gamma = 50$, $N = 50$ and 400

regarding the number of peaks and the location of the peaks. Also, there is quantitative agreement regarding the number of charges in each shell (not shown). However, the HNC and AHNC results give very different heights and widths of the peaks themselves. Comparison to the MC results makes it clear that the bridge function effects are important at this value of the coupling constant. Similar improvement has been illustrated for $\Gamma = 20$ and 40 for several values of N [9].

It remains to explore how well this approach extends to still larger values of Γ , motivated by its possible utility to study freezing into a spherical crystal. As a first step in that direction results are presented and discussed here for $\Gamma = 50, 100$. Figure (2) shows the density profile at $\Gamma = 50$ for two quite different particle numbers $N = 50$ and $N = 400$. For small enough particle number, $N \lesssim 20$, there is only one shell of finite radius near the point at which the density vanishes [3]. The latter is fixed by the condition that the Coulomb force on a test charge balances that of the trap, i.e. $r_{max} = N^{1/3}$. A second shell is present at $N = 50$, while three additional shells are observed for $N = 400$ (as well as a population at the origin [4]). The agreement between MC and AHNC is seen to be quite good in both cases except at very small r for which the both HNC and AHNC fail even at moderate coupling.

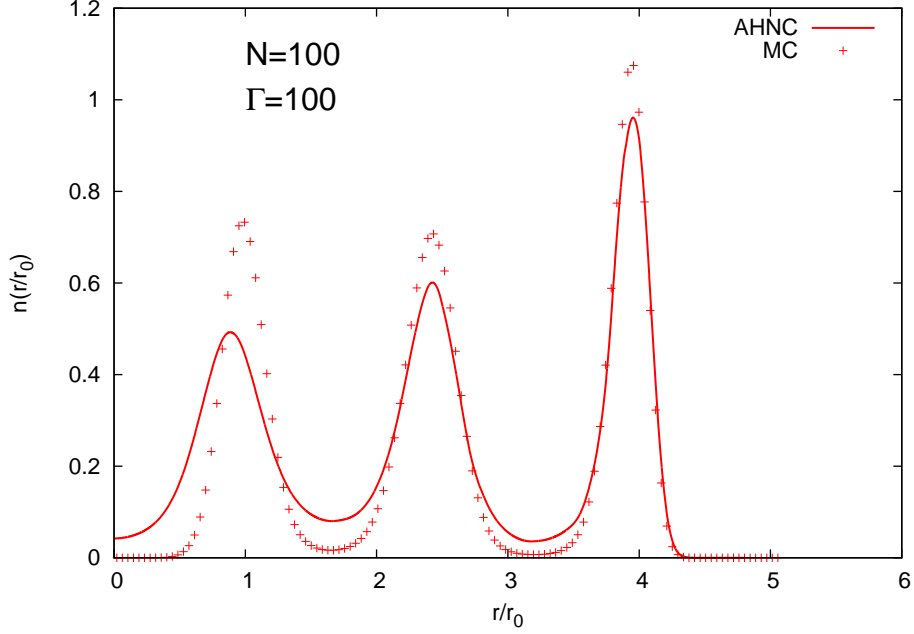


FIG. 3: Comparison of density profile for AHNC and MC results for $\Gamma = 100$ and $N = 100$.

The discrepancies in amplitudes increase somewhat at very strong coupling. This is illustrated in Figure (3) showing the comparison of MC and AHNC results for $\Gamma = 100$, $N = 100$. The error in peak height grows from about 10% for the outer shell to about 30% for the inner shell. Still the overall agreement remains quite good. To explore the conditions for freezing into spherical crystals, even stronger coupling conditions, $\Gamma \sim 200$ are expected to be relevant. However, several important features of the crystal ground state are already evident from the fluid phase AHNC results at the coupling conditions studied. Figure (4) shows a comparison of shell populations from ground state annealed MD simulations [2] with those from AHNC. The latter have been computed for $20 \leq \Gamma \leq 100$, showing a very weak dependence on coupling strength. This is somewhat unexpected since the amplitudes and widths of the shells are quite sensitive to Γ . The shell populations and appearance of shells is clearly quite similar in the fluid and crystal phases. Figure (5) shows a corresponding comparison of shell locations as a function of N . Again the results are remarkably close for both fluid and crystal phases.

The results for the ground state shown on Figures (4) and (5) can be understood theoretically on the basis of a shell model. This represents the density as a sum of delta functions

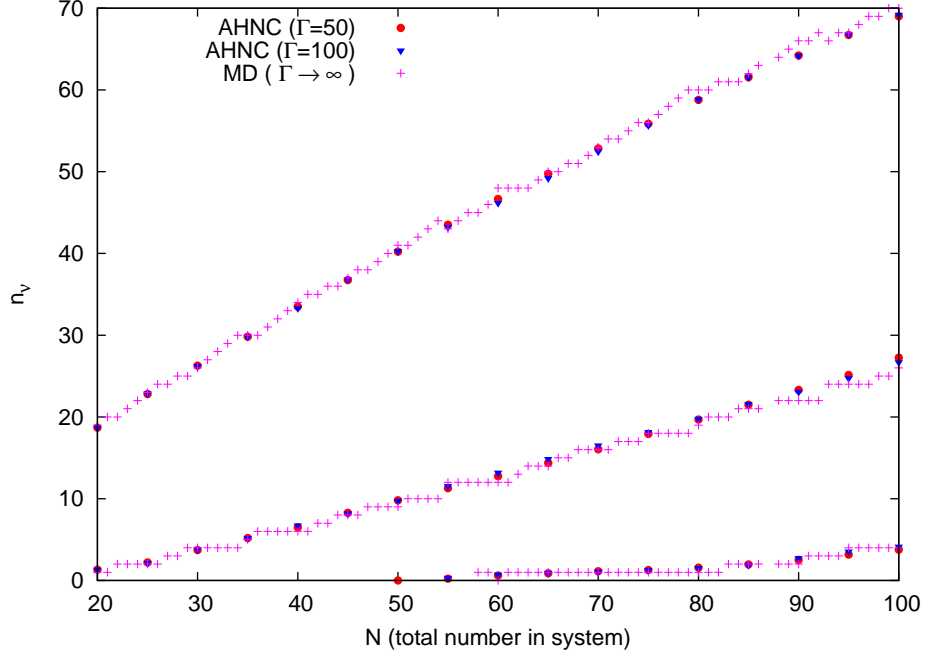


FIG. 4: Comparison of shell populations from AHNC and MD as a function of particle number N .

for particle positions on shells of radii r_ν and occupancy n_ν

$$n(\mathbf{r}) = \sum_{\nu} n_{\nu} \frac{1}{4\pi r_{\nu}^2} \delta(r - r_{\nu}), \quad \sum_{\nu} n_{\nu} = N. \quad (7)$$

The values of n_ν, r_ν are determined by minimizing the total energy [6, 7]. A very accurate representation of the energy for this purpose is constructed on the basis of solutions to the Thomson problem [14] for ground state configurations of Coulomb charges on a single sphere [8]. The intrashell energy is chosen as the known Thomson energy for each n_ν, r_ν , while the intershell energy is taken as the monopole interactions for charges at the corresponding Thomson positions for each shell. In this way the crystal energy, shell populations, and locations are given very accurately. This opens the possibility to test free energies associated with (3) and (4) for broken rotational invariance using parameterized densities similar to the shell model (e.g., Gaussians centered at the Thomson positions) to identify a freezing transition.

This work is supported by the Deutsche Forschungsgemeinschaft via SFB-TR 24, and by the NSF/DOE Partnership in Basic Plasma Science and Engineering under the Department

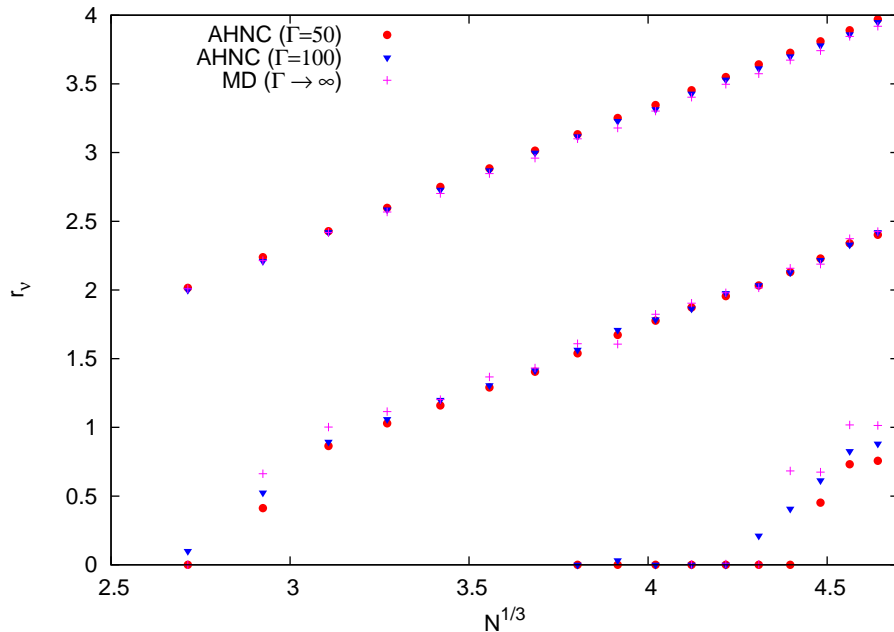


FIG. 5: Comparison of shell radii from AHNC and MD as a function of particle number N .

of Energy award DE-FG02-07ER54946.

-
- [1] T. Pohl, T. Pattard, and J.M. Rost, Phys. Rev. Lett. **92**, 155003 (2004).
 - [2] O. Arp, D. Block, A. Piel, and A. Melzer, Phys. Rev. Lett. **93**, 165004 (2004); O. Arp, D. Block, M. Bonitz, H. Fehske, V. Golubnychiy, S. Kosse, P. Ludwig, A. Melzer, and A. Piel, J. Phys. Conf. Series **11**, 234 (2005).
 - [3] P. Ludwig, S. Kosse, and M. Bonitz, Phys. Rev. E **71**, 046403 (2005).
 - [4] M. Bonitz, D. Block, O. Arp, V. Golubnychiy, H. Baumgartner, P. Ludwig, A. Piel, and A. Filinov, Phys. Rev. Lett. **96**, 075001 (2006).
 - [5] V. Golubnychiy, H. Baumgartner, M. Bonitz, A. Filinov, and H. Fehske, J. Phys. A: Math. Gen. **39**, 4527 (2006).
 - [6] H. Baumgartner, H. Kählert, V. Golubnychiy, C. Henning, S. Käding, A. Melzer, and M. Bonitz, Contrib. Plasma Phys. **47**, 281 (2007); H. Baumgartner, D. Asmus, V. Golubnychiy, P. Ludwig, H. Kählert, and M. Bonitz, New Journal of Physics **10**, 093019 (2008).
 - [7] W. D. Kraeft and M. Bonitz, J. Phys. Conf. Ser. **35**, 94 (2006).

- [8] J. Cioslowski and E. Grzebielucha, *Phys. Rev E* **78**, 026416 (2008).
- [9] J. Wrighton, J. W. Dufty, H. Kählert, and M. Bonitz. “Theoretical Description of Coulomb Balls – Fluid Phase”, arXiv:0909.0775.
- [10] R. Evans, in *Fundamentals of Inhomogeneous Fluids*, edited by D. Henderson (Marcel Dekker, NY, 1992).
- [11] K. C. Ng, *J. Chem. Phys.* **61**, 2680-2689 (1974).
- [12] Y. Rosenfeld and N. W. Ashcroft, *Phys. Rev. A* **20**, 1208 (1979).
- [13] J. P. Schiffer, *Phys. Rev. Lett.* **88**, 205003 (2002).
- [14] J. J. Thomson, *Philos. Mag.* **7**, 237 (1904).